Discrete dislocation dynamics simulation of cutting of γ′ precipitate and interfacial dislocation network in Ni-based superalloys

Yashiro, Kisaragi ; Kurose, F ; Nakashima, Y ; Kubo, K ; Tomita, Yoshihiro ; Zbib, H M

(Citation)
International Journal of Plasticity,22(4):713-723

(Issue Date)
2006-04

(Resource Type)
journal article

(Version)
Accepted Manuscript

(URL)
https://hdl.handle.net/20.500.14094/90000013

Discrete Dislocation Dynamics Simulation of Cutting of γ' Precipitate and Interfacial Dislocation Network in Ni-Based Superalloys

K. Yashiro[a,*], F. Kurose[b], Y. Nakashima[b],

K. Kubo[b], Y. Tomita[a] and H. M. Zbib[c]

[a] *Faculty of Engineering, Kobe University, 1-1, Nada, Kobe 657-8501, JAPAN*

[b] *Student of Graduate School of Engineering, Kobe University, 1-1, Nada, Kobe 657-8501, JAPAN*

[c] *School of Mechanical and Materials Engineering, Washington State University, Pullman, WA, 99164-0000 USA*

Abstract

We proposed a back force model for simulating dislocations cutting into a γ' precipitate, from the physical viewpoint of work for making or recovering an antiphase boundary (APB). The first dislocation, or a leading partial of a superdislocation, is acted upon by a back force whose magnitude is equal to the APB energy. The second dislocation, or a trailing partial of a superdislocation, is attracted by the APB with a force of the same magnitude. The model is encoded in a 3D discrete dislocation dynamics (DDD) code and demonstrates that a superdislocation nucleates after two dislocations pile up at the interface and that the width of dislocations is naturally balanced by the APB energy and repulsion of dislocations. The APB energy adopted here is calculated by *ab-initio* analysis on the basis of the density functional theory (DFT). Then we applied our DDD simulations to more complicated cases, namely,

dislocations near the edges of a cuboidal precipitate and those at the γ/γ' interface covered by an interfacial dislocation network. The former simulation shows that dislocations penetrate into a γ' precipitate as a superdislocation from the edge of the cube, when running around the cube to form Orowan loops. The latter reveals that dislocations become wavy at the interface due to the stress field of the dislocation network, then cut into the γ' precipitate through the interspace of the network. Our model proposed here can be applied to study the dependence of the cutting resistance on the spacing of dislocations in the interfacial dislocation network.

Key words: Discrete Dislocation Dynamics, Superdislocation, Ni-based Superalloy, Anti-Phase Boundary, Interfacial Dislocation Network

1 Introduction

Ni-based superalloys possess a characteristic microstructure in which cuboidal γ' phases are precipitated in the γ matrix. The size of the precipitates is precisely controlled to aquire the highest heat tolerance; the typical length of a cuboidal precipitate is less than $0.5\,\mu$m and the width of the γ matrix is decreased to a few tens of nanometer in fourth- and higher-generation superalloys. The degree of lattice mismatch between the γ and γ' phases is so small that they form coherent interfaces; however, dislocations are strongly affected by the morphology of the microstructure. Such dislocation behavior has attracted considerable interest for the understanding of the deformation mechanism of superalloys.

* Corresponding author. Tel&Fax: +81-78-803-6303
Email address: yashiro@mech.kobe-u.ac.jp (K. Yashiro).
URL: http://solid.mech.kobe-u.ac.jp/ (K. Yashiro).

Dislocations in the microstructure are carefully observed by transmission electron microscopy and their role in creep resistance is discussed in the overview by Pollock and Argon (1992). Recent computational approaches such as strain gradient crystal plasticity have also suggested significant insights, *e.g.*, dislocation density around a γ' precipitate or cross slip by lattice rotation (Busso and McClintock, 1996; Ohashi, 1998; Busso et al., 2000). It is still difficult, however, to study in more detail the interaction between a dislocation and the γ/γ' interface by experimental observations or continuum computational analysis, since the phenomena involve two completely different length scales (microscale and nanoscale). Therefore atomistic or dislocation dynamics studies are necessary to clarify the dislocation behavior at the γ/γ' interface. From such a viewpoint, we have conducted several molecular dynamics (MD) simulations to determine the fundamental aspect of dislocations at the γ/γ' interface (Yashiro et al., 2002, 2004a). MD simulations, however, cannot treat collective behavior of many dislocations nor thermally activated motions such as a dislocation climb. Thus we are now scaling up our study using discrete dislocation dynamics (DDD) simulation (Yashiro et al., 2004b). In the present study, we derive the back force acting on dislocations cutting into a γ' precipitate from the work required to create or recover an antiphase boundary (APB). DDD simulation for dislocations at a flat γ/γ' interface is implemented with the back force and demonstrates that a superdislocation nucleates after two dislocations pile up at the interface and the width of dislocations is naturally balanced by the APB energy and repulsion of dislocations. We have also applied our DDD simulation to more complicated cases such as dislocations at edges of cuboidal precipitate and those at the γ/γ' interface covered by an interfacial dislocation network. The APB energy adopted is calculated by *ab-initio* analysis based on the density functional theory (DFT).

2 Simulation Procedure

2.1 DDD outline

According to the formulation proposed by Zbib and coworkers (Zbib et al., 1998, 2002), all dislocation lines and loops of arbitrary shapes are discretized into short line segments and the time evolution of each dislocation is determined by calculating the motion of dislocation nodes. Discretization is updated continuously to represent the arbitrary shapes of dislocations. The force acting on node i of the position vector $\mathbf{p}$ is calculated using

$$\mathbf{F}_i = \sum_{j=1}^{N-1} \left(\boldsymbol{\sigma}^{\mathrm{D}}_{j,j+1}(\mathbf{p}) + \boldsymbol{\sigma}^{\mathrm{a}}(\mathbf{p}) \right) \cdot \mathbf{b}_i \times \boldsymbol{\xi}_i + \mathbf{F}_{i-\mathrm{self}} \quad , \tag{1}$$

where $\sigma^{\mathrm{D}}_{j,j+1}(\mathbf{p})$ is the stress at $\mathbf{p}$ generated by a remote segment, $\sigma^{\mathrm{a}}(\mathbf{p})$ the applied stress, and N the number of nodes; $\mathbf{b}_i$ and $\boldsymbol{\xi}_i$ are the Burgers vector and line sense vector at node i, respectively, as shown in Fig. 1. Thus the first term on the right-hand side of Eq. (1) represents the Peach-Koehler (PK) force. $\mathbf{F}_{i-\mathrm{self}}$ is the line tension evaluated by the curvature at node i (Hirth, 1982). The motion of dislocations is traced by solving the following equation of motion numerically.

$$m\dot{\boldsymbol{v}}_i + \frac{1}{M(T,p)}\boldsymbol{v}_i = [\boldsymbol{F}_i]_{\mathrm{glide-component}} \tag{2}$$

Here, $\boldsymbol{v}_i$ is the glide velocity and m the effective mass per unit dislocation; T and p are the temperature and pressure, respectively. M is the mobility accounting for damping effects, such as phonon drag. In the present study, m and M are set to $\rho b^2/2$ and $10^{-2}\,(\mathrm{Pa.s})^{-1}$, respectively, where ρ is the density.

2.2 DDD-FEM coupling

The formulation of $\sigma^{\mathrm{D}}_{j,j+1}(\mathbf{p})$ is defined in the infinite body of a homogeneous material, so that it could not directly be applied to solve problems involving surfaces or heterogeneous interfaces. The superposition principle is used to treat the problem. The displacement $\mathbf{u}$, strain $\boldsymbol{\varepsilon}$, and stress $\boldsymbol{\sigma}$ in a finite body containing a γ' precipitate are given by the sum of the two solutions

$$\mathbf{u}=\mathbf{u}^{\infty}+\mathbf{u}^{*},\ \boldsymbol{\varepsilon}=\boldsymbol{\varepsilon}^{\infty}+\boldsymbol{\varepsilon}^{*},\ \boldsymbol{\sigma}=\boldsymbol{\sigma}^{\infty}+\boldsymbol{\sigma}^{*} \quad , \tag{3}$$

where ∞ implies the solution of DDD analysis for the domain V in an infinite homogeneous body, while $*$ that of FEM for a finite body with a volume V. In the FEM analysis, the following constitutive equations are defined for the matrix and precipitate, respectively.

$$\begin{aligned} \boldsymbol{\sigma}^{*}&=\mathbf{C}^{\mathrm{m}}\boldsymbol{\varepsilon}^{*} && \text{in } V_{\mathrm{m}} \\ \boldsymbol{\sigma}^{*}&=\mathbf{C}^{\mathrm{p}}\boldsymbol{\varepsilon}^{*}+[\mathbf{C}^{\mathrm{p}}-\mathbf{C}^{\mathrm{m}}]\boldsymbol{\varepsilon}^{\infty} && \text{in } V_{\mathrm{p}} \end{aligned} \tag{4}$$

Here, $\mathbf{C}^{\mathrm{m}}$ and $\mathbf{C}^{\mathrm{p}}$ are the elastic stiffnesses of the matrix and precipitate, V_{m} and V_{p} are the volumes of the matrix and precipitate in the finite body V, respectively. The second term of the lower equation is the "eigenstress". The boundary conditions are

$$\begin{aligned} \mathbf{t}^{*} &= \mathbf{t}^{\mathrm{a}}-\mathbf{t}^{\infty} && \text{on} && \partial V \quad , \\ \mathbf{u}^{*} &= \mathbf{u}^{\mathrm{a}} && \text{on} && \text{part of } \partial V \quad , \end{aligned} \tag{5}$$

where $\mathbf{t}^{\mathrm{a}}$ is the externally applied traction while $\mathbf{t}^{\infty}$ is the traction caused by dislocations resulting from the infinite-homogeneous-domain problem.

2.3 Back force in precipitate

When a dislocation cuts into or glides in a γ' precipitate, it leaves an antiphase boundary on the slip plane. Thus, an excess energy equal to the APB energy of the swept area is necessary to cut into or move in the precipitate. Consider a straight segment of length L that travels normal to the segment at a distance n. The APB energy of the swept area is expressed as

$$E_{\mathrm{APB}} = \chi_{\mathrm{APB}} L n \quad , \tag{6}$$

where χ_{APB} is the inherent APB energy per unit area. Assume that the back force on dislocation is constant in the precipitate. Then the work performed by the dislocation is written as

$$W = F_b L n \quad , \tag{7}$$

where F_b is the back force per unit length. Comparing Eqs.(6) and (7), we obtain $F_b = \chi_{\mathrm{APB}}$. The unit of the energy per area is converted to that of force per length as J/m^2=Nm/m^2=N/m. When the next position of a dislocation node i is in the area of γ' precipitate, or the dislocation expands the APB, the node receives a repulsive force of F_b. On the other hand, the follow-on dislocation gliding in the APB receives an attractive force of F_b to dissolve the APB. This back force model is schematically illustrated in Fig. 2.

2.4 Simulation models

The back force condition is encoded in the DDD-FEM simulation package, that is, multiscale dislocation dynamics plasticity (MDDP), developed by Zbib et al. (2002). All the short-range interactions of dislocations, such as annihilation,

junction and jog formation, are included in the DDD package. Three simulation models are considered in this study. The first, referred to as Model 1, employs a cubic cell made of γ and γ' layers, as shown in Fig. 3. The cell is $1.13\,\mu$m $\times$ $1.13\,\mu$m $\times$ $1.13\,\mu$m, and each of its layers has the same thickness of $0.57\,\mu$m. The shear moduli of the γ and γ' phases are set to 80 GPa and 85 GPa, respectively. Poisson's ratio is set to 0.3 for both phases. Two Frank-Read (FR) sources whose Burgers vector is $[01\bar{1}]$ are set on the same (111) slip plane, as schematically shown in the figure. The source near the interface has a width of $1.51\,\mu$m ($6040b$, b is the magnitude of Burgers vector) while the other source $0.21\,\mu$m ($800b$). To accelerate the propagation of dislocation loops and bring dislocations to the interface, a uniform stress of 500 MPa is applied in the z-direction in the DDD analysis. In the FEM analysis, the cell is divided into $10 \times 10 \times 10$ cubic elements and subjected to the loading conditions shown in Fig. 3(b). Here, the periodic boundary condition tends to significantly multiply dislocations in the γ matrix and easily leads overloads of computation, so that we adopt the free boundary condition in which dislocations receive the image force near the surface.

The second simulation model, Model 2, is implemented with a cubic cell containing a cuboidal precipitate, as shown in Fig. 4. The cell is $2.51\,\mu$m in length while the precipitate is $0.84\,\mu$m in length. An FR source is set beneath the precipitate and a dislocation is propagated from the source and approaches the precipitate under a tensile stress of 500MPa. The Burgers vector and the width of the FR source are $[\bar{1}01]$ and $0.35\,\mu$m ($1400b$), respectively. $9 \times 9 \times 9$ cubic elements are used in FEM. The boundary condition, shear moduli and Poisson's ratio are the same as those of Model 1. The misfit stress around the cuboidal precipitate is not considered in the present study, so that we

investigate the different behavior of dislocations at a flat surface and edges of cuboidal precipitate depending only on the back-force.

The last simulation model, Model 3, is for describing the interaction between an interfacial dislocation network and approaching dislocations. All the simulation conditions of Model 3 is identical to those of Model 1, but 5×5 straight dislocations are arranged at the γ/γ' interface, as shown in Fig. 5. The slip plane of the FR source crosses just at the intersections of the dislocation network. The Burgers vectors of the network dislocations are defined experimentally (Zhang et al., 2002). It is also revealed that the intersections have different Burgers vectors, however, we simplify the network by removing any intersections. The dislocation spacing of the network is set to $0.23\,\mu$m ($900b$).

The APB energy χ_{APB} is set to $126\,\mathrm{mJ/m^2}$ in all the simulations. χ_{APB} is evaluated using the Vienna ab-initio simulation program (VASP, Kresse and Hafner, 1993) with ultrasoft pseudopotential and generalized gradient approximation (GGA). 2, 4 and 8 unit lattices of Ni_3Al are stacked as supercells and two APB planes are introduced in the supercells. χ_{APB} is evaluated by the energy increase of these supercells from the reference energy of a perfect single crystal. $\boldsymbol{k}$-points of $8 \times 8 \times 3 \sim 8 \times 8 \times 1$ and a cutoff energy of $241.62\,\mathrm{eV}$ are used in the calculations.

3 Results and Discussions

3.1 Nucleation of superdislocation

Figure 6 shows the dislocation motion in the simulation of Model 1. There is the γ' phase in the lower half of the cell although it is not indicated in the figure. The time increment $\Delta t = 10^{-11}$ s is used in the numerical integration of Eq. (2). The first dislocation from the larger FR source piles at the interface quickly. The second dislocation that propagates from the shorter FR source is also blocked at the interface by the repulsive force from the first dislocation, and straightened along the interface during $t = 200 \sim 500\Delta t$. The pair of these dislocations, however, cannot penetrate into the γ' phase at this stage despite an applied external stress of $\sigma_{zz} = 500$ MPa. When the third dislocation is generated by multiplication at the shorter FR source and approaches the dislocation pair, the pair begins to cut into the γ' phase and form a superdislocation ($t = 800 \sim 900\Delta t$). Once the superdislocation nucleates, it goes through the γ' phase as fast as the dislocations in the γ phase since the repulsive and attractive back forces cancel out each other and the shear moduli of both phases are almost same. The "superpartial"s maintain a constant distance in the γ' phase and their width is about 13 nm ($52b$). The third dislocation piles at the interface again at $t = 1000\Delta t$ (Fig. 6(f)). This motion of dislocations is quantitatively indicated in Fig. 7. The abscissa is the time step, and the ordinate the distance from the interface evaluated at the forefront of dislocation loops. The first and second dislocations pile at the interface and maintain a constant distance until the third dislocation approaches. Then the first dislocation cuts into the γ' phase at about $t = 900\Delta t$ and the second ap-

proaches the interface while keeping its distance to the first dislocation. During this penetration, the velocity of two dislocations is low since the back force of the APB acts only on the first dislocation. That is, in our model, the APB does not generate an attractive force on the trailing dislocation away from the interface, and expands larger than the equilibrium width in the nucleation of a superdislocation. This phenomenon, however, does not conflict with our MD results in which the APB does not attract a trailing dislocation (Yashiro et al., 2004a). When the second dislocation reaches the interface, it receives an attractive force from the APB and increases its velocity, resulting in the decrease in the width of superpartials. The superdislocation glides swiftly in the γ' phase when the trailing superpartial catches up with the leading dislocation and reaches the equilibrium distance in which back forces cancel out.

3.2 Dislocations at Edges of Cuboidal γ' Precipitate

Figure 8 shows the dislocation motion observed in the simulation of Model 2. In the figure, the trigonal cross section of γ' is indicated on the (111) slip plane. The first dislocation faces the bottom of γ' and is blocked there at $t = 300\Delta t$ (Fig. 8(b)). Then the dislocation runs around the cuboidal precipitate to form Orowan loop at $t = 400 \sim 700\Delta t$ (Figs. 8(c),(d)). The dislocation slightly intrudes in γ' at the edge without a trailing dislocation but with the line tension. This is consistent with the MD results (Yashiro et al., 2002). The second dislocation is generated at the FR source and piles at the bottom of γ' (Figs. 8(c),(d)). Due to the characteristic of the Burgers vector, the dislocation loop reaches the right edge of the trigonal cross section slightly to the left, and receives an attractive force from the APB at the edge. Thus a superdislocation

nucleates at the right edge and glides in the γ' precipitate (Figs. 8(e),(f)). It is natural that the superdislocation cuts into the γ' precipitate from the edge, which is supported by our MD results (Yashiro et al., 2004a).

3.3 Interfacial Dislocation Network

Finally, we show the dislocation motion near the interfacial dislocation network in Fig. 9. The first dislocation swiftly piles at the interface despite the presence of network dislocations (Fig. 9(a)). The second dislocation also piles at the interface, however, the shape becomes wavy due to the stress field from the network (Fig. 9(b)). In Fig. 9(c), we can find that the third dislocation approaches the interface and piles there without nucleating the superdislocation. The dislocations cut into the γ' phase when the fourth dislocation is generated at the FR source and they push forward the dislocation pair, as shown in Fig. 9(d). Thus the resistance against penetration is increased by the dislocation network. Figure 9(d) also suggests that the dislocations penetrate into the γ' phase from the interspace of the dislocation net. The dislocations are also pinned and bowed out by the network dislocation; however, this is debatable since the short-range interaction between misfit dislocations at the interface and dislocations in the γ or γ' is not modeled yet. In addition, the stress field of this network, composed of dislocations in the γ phase, is much stronger than those of the network made of misfit dislocations. This difference, however, can be treated by putting the internal positive/negative stress on the γ' phase in FEM.

4 Conclusion

To simulate dislocation behavior at the γ/γ' interface, a back force model for discrete dislocation dynamics (DDD) simulation is proposed according to the work for making/recovering an antiphase boundary (APB). Dislocation nodes cutting/gliding in the γ' phase receive a repulsive back force equal to χ_{APB}, the APB energy per unit area, to leave the APB on the slip plane. On the other hand, nodes on a trailing dislocation receive an attractive back force of the same magnitude to dissolve the APB. We first evaluate a χ_{APB} of $126\,\mathrm{mJ/m^2}$ by *ab-initio* calculation based on the DFT-GGA (density functional theory - generalized gradient approximation) ultrasoft pseudopotential method. The APB energy is encoded in the DDD simulation package proposed by Zbib et al. (1998, 2002) as the back force condition. It is demonstrated that a superdislocation nucleates after two dislocations pile up at the interface and that the width of superpartials is naturally balanced by the APB energy and repulsion of dislocations. We applied our DDD simulation to more complicated phenomena, namely, dislocations at the edges of a cuboidal γ' precipitate and those approaching the interfacial dislocation network. The former shows that dislocations cut into the γ' cube from the edge during forming Orowan loops. The latter suggests that cutting resistance is increased by the network and they cut into the γ' phase from the interspace of the dislocation net.

Acknowledgment

This work was supported financially in part by a Grant-in-Aid for Scientific Research from the Ministry of Education, Culture, Sports, Science and Tech-

nology of Japan.

References

Busso, E. P. and McClintock, F.A., 1996. A Dislocation Mechanics-Based Crystallographic Model of a B2-Type Intermetallic Alloy. Int. J. Plasticity, Vol.12, pp.1-28.

Busso, E. P., Meissonnier, F., and O'Dowd, N. P., 2000. Gradient-Dependent Visco-Plastic Deformation of Two-Phase Single Crystals. J. Mech. Phys. Solids, V. 48, pp. 2333-2361.

Hirth, J. P. and Lothe, J., 1982. Theory of Dislocations, second ed., John Wiley & Sons.

Kresse, G. and Hafner, J., 1993. Ab Initio Molecular Dynamics for Liquid Metals. Phys. Rev. B, Vol. 47, pp.558–561.

Ohashi, T., 1998. "Evaluation and Visualization of Geometrically Necessary Dislocations in Metal Microstructures by means of Continuum Mechanics Analysis. Journal de Physique IV, 9, pp.279-284.

Pollock, T. M. and Argon, A. S., 1992. Creep Resistance of CMSX-3 Nickel Base Superalloy Single Crystals. Acta Metal. Mater., Vol. 40, pp. 1–30.

Yashiro, K., Naito, M. and Tomita, Y., 2002. Molecular Dynamics Simulation of Dislocation Nucleation and Motion at γ/γ' Interface in Ni-Based Superalloy. Int. J. Mech. Sci., Vol. 44, pp. 1845-1860.

Yashiro, K., Tabata, Y. and Tomita, Y., 2004a. Molecular Dynamics Study on the Characterisitics of Edge and Screw Dislocations in Gamma/Gamma-Prime Microstructure in Ni-based Superalloy. IUTAM Symposium on Mesoscopic Dynamics of Fracture Process and Material Strength, Eds. Kitagawa, H. and Shibutani, Y., pp.59–68.

Yashiro, K., Tabata, Y., Kurose, F., Tomita, Y. and Zbib, H. M., 2004b. MD / DDD Study on Dislocation Behaviors at Matrix-Precipitate Interface in Nickel-Based Superalloys. MMM-II Conference Proceedings, pp.169–172.

Zbib, H. M. Rhee, M. and Hirth, J. P. 1998. On Plastic Deformation and the Dynamics of 3D Dislocations. Int. J. Mech. Sci., Vol. 40, pp. 113-127.

Zbib, H. M. and Diaz de la Rubia, T., 2002. A multiscale model of plasticity. Int. J. Plasticity, Vol. 18, pp. 1133-1163.

Zhang, J. X., Murakumo, T., Koizumi, Y., Kobayashi, T., Harada, H. and Masaki Jr., S., 2002. Interfacial Dislocation Networks Strengthening a Fourth Generation Single-Crystal TMS-138 Superalloy. Metal. Mater. Trans., A, Vol. 33A, pp.3741–3746.

captions.

Fig. 1. Nodes and segments on dislocation loops.

Fig. 2. Schematic of back force acting on leading and trailing superpartials.

Fig. 3. Simulation model 1.

Fig. 4. Simulation model 2.

Fig. 5. Interfacial dislocation network model.

Fig. 6. Motion of dislocations in Model 1.

Fig. 7. Normalized position of dislocation forefront in Model 1.

Fig. 8. Motion of dislocations in Model 2.

Fig. 9. Motion of dislocations in Model 3.

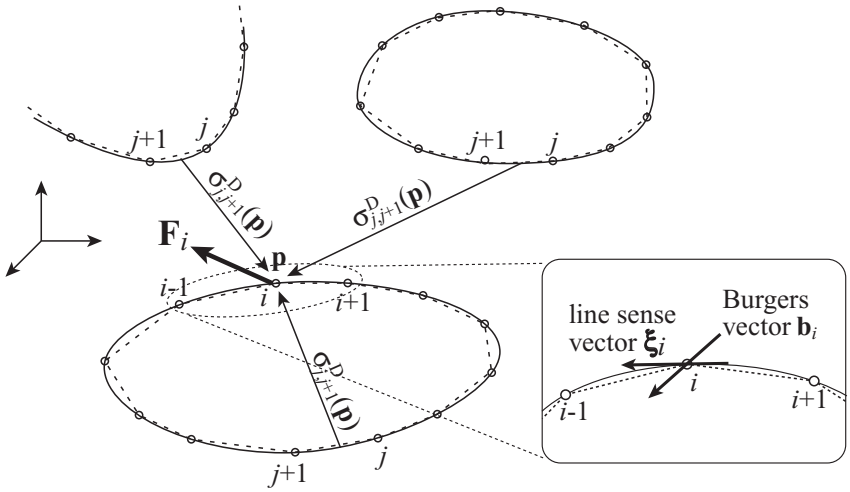

Fig. 1.

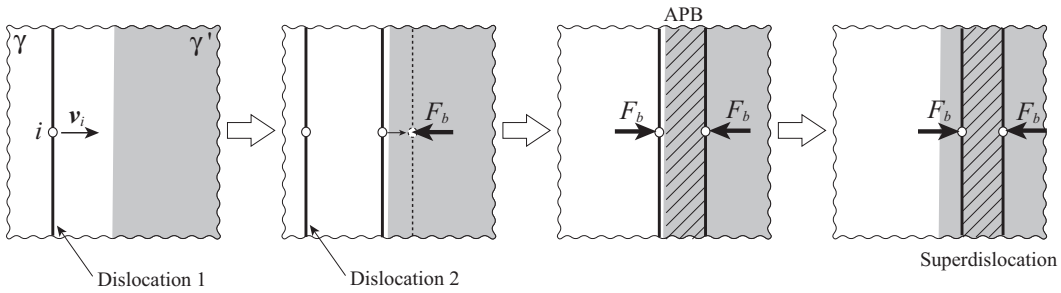

Fig. 2.

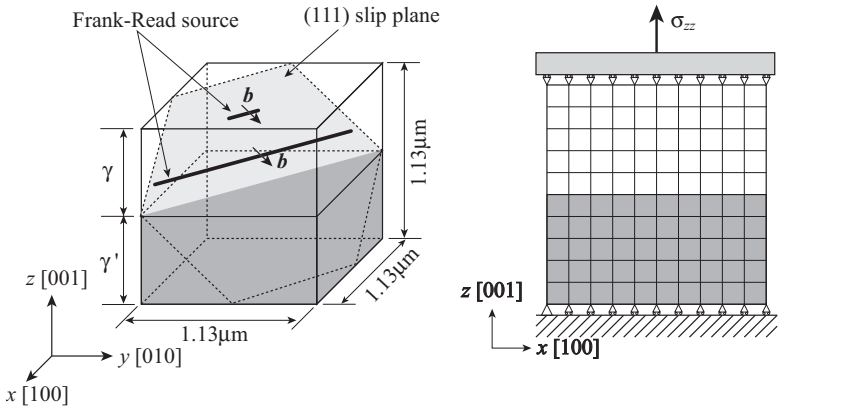

(a) Dimensions of simulation cell (b) Loading condition and FEM mesh

Fig. 3.

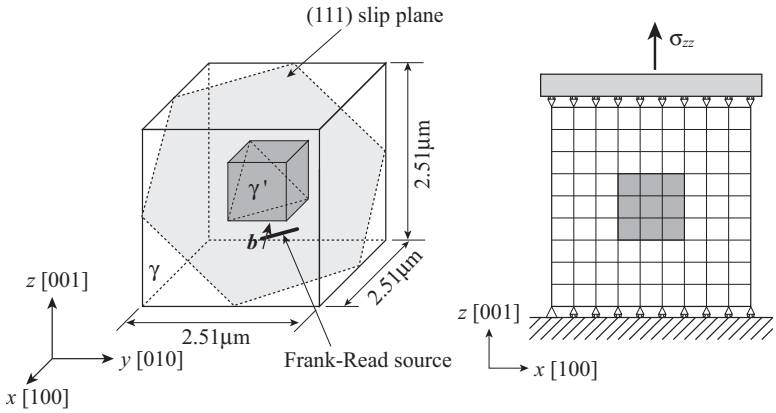

(a) Dimensions of simulation cell (b) Loading condition and FEM mesh

Fig. 4.

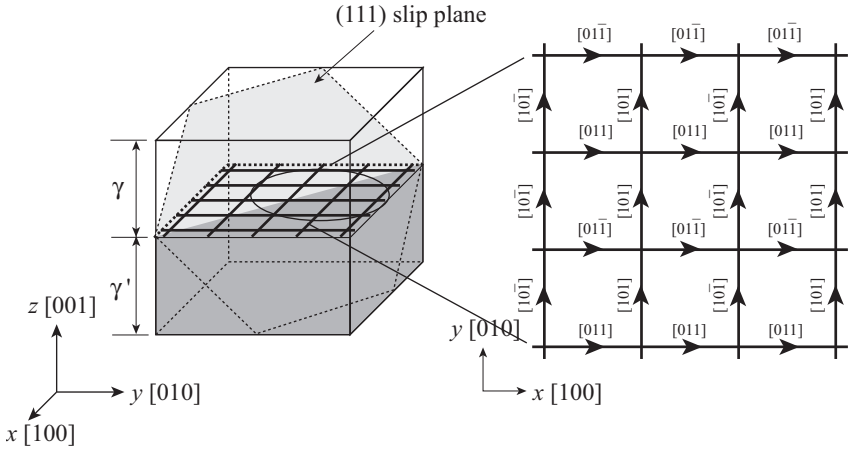

Fig. 5.

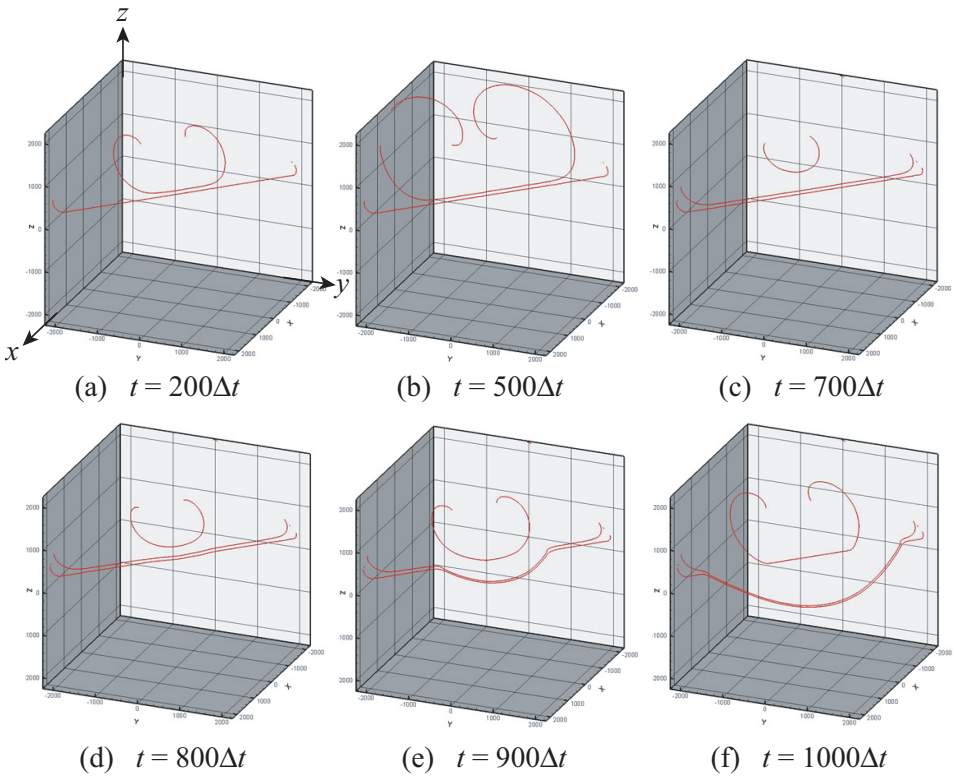
z
y
x
(a) $t = 200\Delta t$
(b) $t = 500\Delta t$
(c) $t = 700\Delta t$
(d) $t = 800\Delta t$
(e) $t = 900\Delta t$
(f) $t = 1000\Delta t$

Fig. 6.

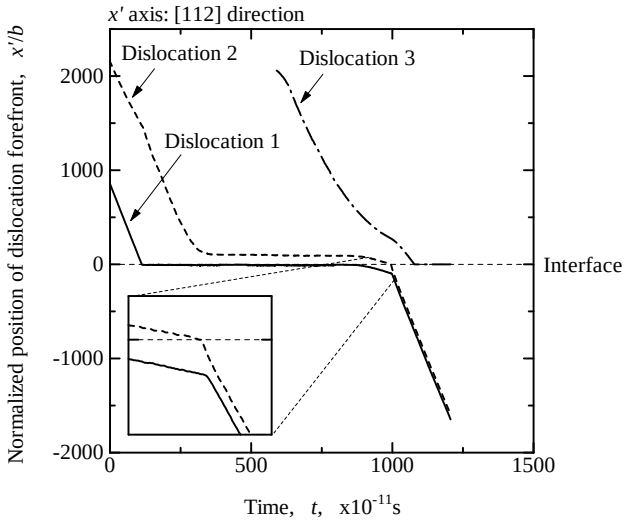
x′ axis: [11$\bar{2}$] direction
Dislocation 2
Dislocation 3
Dislocation 1
Interface
Normalized position of dislocation forefront, x′/b
Time, t, x10^{-11}s
2000
1000
0
-1000
-2000
0
500
1000
1500

Fig. 7.

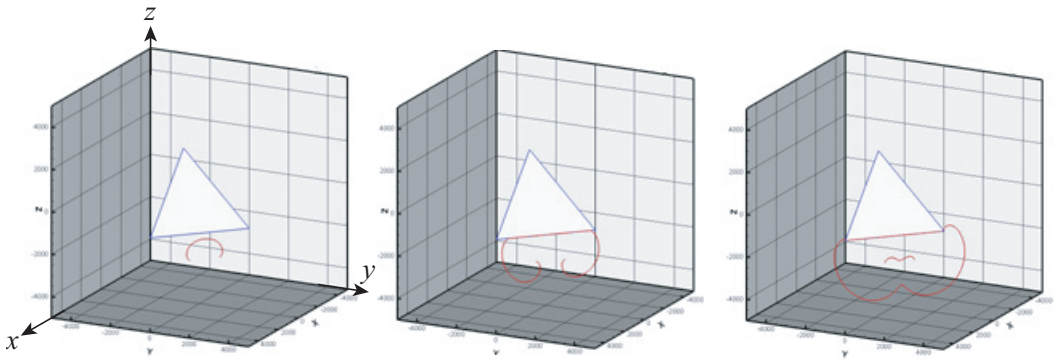

(a) $t = 100\Delta t$ (b) $t = 300\Delta t$ (c) $t = 400\Delta t$

(d) $t = 700\Delta t$ (e) $t = 860\Delta t$ (f) $t = 950\Delta t$

Fig. 8.

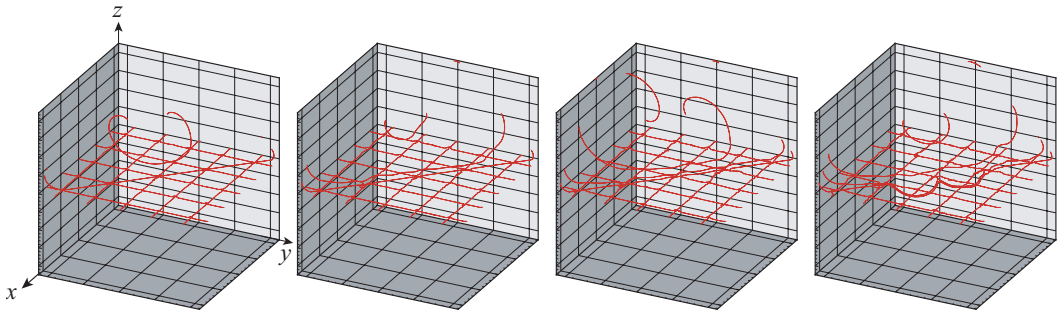

(a) $t = 300\Delta t$ (b) $t = 900\Delta t$ (c) $t = 1500\Delta t$ (d) $t = 1800\Delta t$

Fig. 9.